Springer

KSME

Journal of Mechanical Science and Technology 26 (4) (2012) 1171~1177
www.springerlink.com/content/1738-494x
DOI 10.1007/s12206-012-0219-8

Design and simulation for a hydraulic actuated quadruped robot †

Xuewen Rong[1], Yibin Li[1,*], Jiuhong Ruan[2] and Bin Li[1]

[1]*School of Control Science and Engineering, Shandong University, Jinan, 250061, China*
[2]*Advanced Vehicle and Robot Institute, Shandong Jiaotong University, Jinan, 250031, China*

(Manuscript Received March 25, 2011; Revised December 7, 2011; Accepted December 19, 2011)

Abstract

This paper describes the mechanical configuration of a quadruped robot firstly. Each of the four legs consists of three rotary joints. All joints of the robot are actuated by linear hydraulic servo cylinders. Then it deduces the forward and inverse kinematic equations for four legs with D-H transformation matrices. Furthermore, it gives a composite foot trajectory composed of cubic curve and straight line, which greatly reduces the velocity and acceleration fluctuations of the torso along forward and vertical directions. Finally, dynamics co-simulation is given with MSC.ADAMS and MATLAB. The results of co-simulation provide important guidance to mechanism design and parameters preference for the linear hydraulic servo cylinders.

Keywords: Co-simulation; D-H transformation; Kinematics; MSC.ADAMS; Quadruped robot; Trot gait

1. Introduction

Wheeled robots can travel very fast, but they usually require a fairly flat floor over which to work. Tracked robots can move on rougher terrain, but slower than wheeled robots. Legged robots are superior to wheeled and tracked robots since they have higher terrain adaptivity, possess greater mobility and flexibility, do little damage to the environment, etc. Nevertheless, legged robots are more complicated in structure and difficult to control than wheeled or tracked robots. The theories concerning legged robots are still in the development stage.

During the last four decades, walking (or legged) robots have been an exciting research field. Many improvements have been made since the first full computer-controlled robot "Phoney Pony" was made at the University of Southern California in 1966 [1]. Since then, a large number of walking robots, such as BISAM [2], WARP1 [3], KOLT [4], Tekken [5], HuboDog [6], p2 [7], HyQ [8], etc., have been developed all over the world. Up to now, the most advanced walking robot is BigDog [9] made by Boston Dynamics in 2008. BigDog and p2 adopt linear and rotary hydraulic cylinders to drive the articular joints, respectively. HyQ adopts geared motors to drive the rolling joints and linear hydraulic cylinders to drive the pitching joints respectively. Others adopt electric motors to drive all joints.

Compared to an electric motor driving system powered by batteries, the hydraulic driving system powered by an engine has several important advantages:

- Higher power-to-mass ratio, which makes the robot more compact and with larger load capability.
- Greater endurance.
- More quickly refueled than recharged.
- Faster dynamic response, which makes the robot more stable.
- Better load stiffness, which reduces the effect caused by varied payload or other external force disturbance.
- More convenient to distribute driving energy to joints according to actual needs.

We have done a great deal of work on mechanical structure, kinematics and dynamics simulation for hydraulic actuated quadruped robots [10]. A four-legged robot with four degrees of freedom (DOFs) per leg has kinematic redundance and better adaptability to uneven terrain. But its mechanical structure, motions planning and control algorithm are more complex than those of a robot with three DOFs per leg. So we preferred to make a physical quadruped robot named Scalf-1 with three DOFs per leg to do many experimental studies. If the link parameters a_2 and θ_2 in Ref. [10] are set to zero, the mechanical structures of four legs are identical to those of the legs of Scalf-1. So the results in Ref. [10] are directly applied to this paper. Scalf-1 weighs about 65 kg without hydraulic power pack and can run at the velocity of 1.8 m/s with trot gait on flat ground in experiments.

*Corresponding author. Tel.: +86 0531 88396813, Fax.: +86 0531 88396813
E-mail address: liyb1960@163.com
† Recommended by Associate Editor Sangyoon Lee

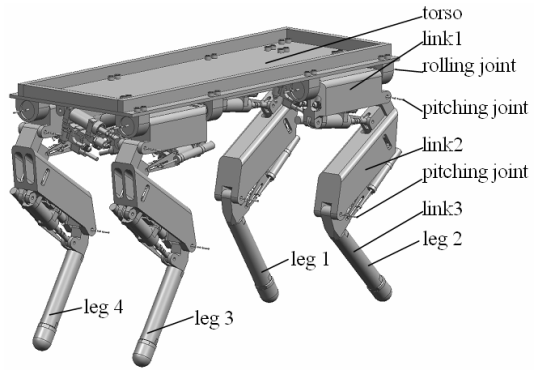

Fig. 1. Three-dimensional prototype of Scalf-1.

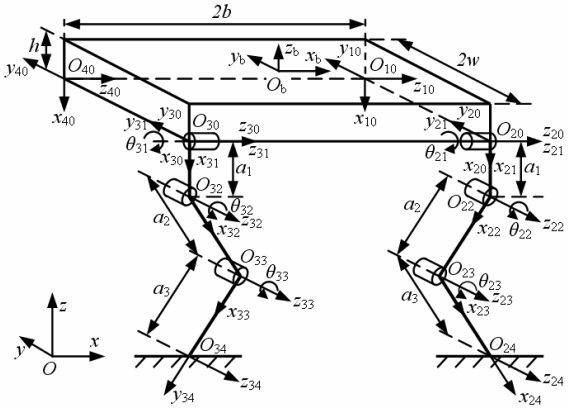

Fig. 2. D-H coordinate frames of Scalf-1.

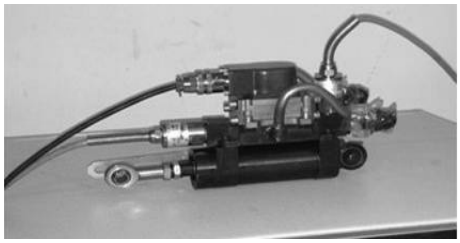

Fig. 3. Linear hydraulic servo cylinder.

2. Mechanism design

As shown in Fig. 1, each leg of the robot has a rolling rotary joint and two pitching rotary joints. The joints topology is shown in Fig. 2. All 12 joints are actuated by identical linear hydraulic servo cylinders illustrated in Fig. 3, each of which is composed of one single rod cylinder, one servo valve, one displacement and two pressure sensors.

The stride frequency is a significant specification of the quadruped robot, which plays an important role in the dynamic stability of the robot. Running with higher stride frequency, the robot is more stable, but it requires high response frequency of the hydraulic servo cylinders. Ref. [11] has discussed the relationships between the energic costs and stride frequency. How speed and stride frequency change with body size from 30 g mice to 680 kg horses has been studied in Refs. [12, 13], which shows that the stride frequency of quadrupedal mammals decreases with increasing body size and increases with increasing running speed. High stride frequencies are less efficient. The objective mass of our quadruped robot is no larger than 120 kg with power pack and the objective speed is no less than 1.5 m/s. Allow for Refs. [11-13], the optimal stride frequency of our quadruped robot is 1 Hz to 3 Hz. The response frequency of hydraulic servo cylinders must meet the requirement of stride frequency.

Table 1. Summary of the major specifications of Scalf-1.

Specifications	Values
Weight (without power pack)	about 65 kg
Dimensions (L × W × H)	1 m × 0.4 m × 0.68 m
DOFs per leg	3 active (rotary)
Hydraulic pressure	21 MPa
Major locomotion gait	trot
Optimal stride frequency	1 Hz to 3 Hz
Max. payload on flat ground	80 kg
Max. velocity on flat ground	1.8 m/s
Max. dynamic force of cylinder	about 3700 N

Table 2. Link parameters of Scalf-1.

Link k	a_{k-1}	α_{k-1}	Joint variables		Theoretical range of θ_{ik}	
			d_{ik}	θ_{ik}	Fore legs	Rear legs
1	0	0°	0	θ_{i1}	(-90°, 90°)	
2	a_1	90°	0	θ_{i2}	(0°, 90°)	(-90°, 0°)
3	a_2	0°	0	θ_{i3}	(-180°, 0°)	(0°, 180°)
4	a_3	0°	0	/	/	/

The major specifications of Scalf-1 are listed in Table 1. Among them, the maximum dynamic force and total oil flow of the hydraulic cylinders are determined according to the dynamics simulation which will be discussed later.

3. Kinematic equations

3.1 D-H coordinate frames and link parameters

As shown in Fig. 2, the origin of the body fixed coordinate frame $\{O_b\}$ is located in the geometric center of the torso, and x_b points to the forward direction, z_b points opposite to the gravity direction. There are four coordinate frames noted as $\{O_{i0}\}$ (i =1, 2, 3, 4) fixed on the four corners of the torso, respectively. The coordinate frames fixed on link k noted as $\{O_{ik}\}$ of four legs are established according to D-H rules [14]. The subscripts i and k are the sequence numbers of four legs and links. Since the mechanical configurations of the legs are extremely identical, the coordinate frames and transformation matrices of four legs are identical too. The only difference is the posture between forelegs and rear legs. The link parameters of Scalf-1 are illustrated in Fig. 2 and listed in Table 2.

3.2 Forward kinematic equations

Since four legs of Scalf-1 have the same D-H coordinate frames and link parameters, they have same forward kinematic equations from $\{O_{i4}\}$ to $\{O_{i0}\}$. The transformations from $\{O_{i0}\}$ to $\{O_b\}$ for four legs can be expressed by the following transformation matrix with different values of δ and λ:

$$ {}^{b}\mathbf{T}_{i0} = \begin{bmatrix} 0 & 0 & 1 & \delta b \\ 0 & 1 & 0 & \lambda w \\ -1 & 0 & 0 & -h \\ 0 & 0 & 0 & 1 \end{bmatrix} \tag{1} $$

where b, w and h are geometry parameters of the torso specified in Fig. 2, δ and λ are sign flags which are defined as below:

$$ \delta = \begin{cases} 1 & i=1, 2 \\ -1 & i=3, 4 \end{cases}, $$

$$ \lambda = \begin{cases} 1 & i=1, 4 \\ -1 & i=2, 3 \end{cases}. $$

The coordinates of one foot with respect to $\{O_{i0}\}$ corresponding to the same leg can be obtained easily through homogeneous transformations. It is given by

$$ {}^{i0}\mathbf{T}_{i4} = \begin{bmatrix} c_1c_{23} & -c_1s_{23} & -s_1 & a_1c_1 + a_2c_1c_2 + a_3c_1c_{23} \\ s_1c_{23} & -s_1s_{23} & c_1 & a_1s_1 + a_2s_1c_2 + a_3s_1c_{23} \\ -s_{23} & -c_{23} & 0 & -a_2s_2 - a_3s_{23} \\ 0 & 0 & 0 & 1 \end{bmatrix} \tag{2} $$

where $c_k = \cos\theta_{ik}$, $s_k = \sin\theta_{ik}$, $c_{23} = \cos(\theta_{i2}+\theta_{i3})$, $s_{23} = \sin(\theta_{i2}+\theta_{i3})$.

Eq. (2) is the forward kinematic equation for four legs. The coordinates of four feet in $\{O_{i0}\}$ can be solved, respectively, from it. Further, the coordinates of four feet in $\{O_b\}$ can be obtained by premultiplying transformation matrix ${}^{i0}\boldsymbol{T}_{i4}$ with ${}^{b}\boldsymbol{T}_{i0}$ respectively.

3.3 Inverse kinematic equations

The inverse kinematic analysis is necessary for motion planning and controlling. Although the forward kinematic equations for four legs from $\{O_{i4}\}$ to $\{O_{i0}\}$ are identical, the inverse kinematic equations of joint variables θ_{i2} and θ_{i3} are not the same since the fore legs and the rear legs are in different postures.

The feet of Scalf-1 are simplified to four points in this paper. If given the coordinates of one foot with $(p_{ix}, p_{iy}, p_{iz}, 1)^T$ in $\{O_{i0}\}$, the corresponding joint variables θ_{ik} can be resolved from the inverse kinematic equations. Moreover, its coordinates in other frames can be obtained by forward and inverse homogenous transformation. Ref. [10] gives the detailed derivation for inverse kinematic equations of a quadruped robot. This paper gives the results directly as follows:

$$ \theta_{i1} = \tan^{-1}\frac{p_{iy}}{p_{ix}}, \tag{3} $$

$$ \theta_{i3} = \pm\cos^{-1}\left(\frac{\left(p_{ix}c_1 + p_{iy}s_1 - a_1\right)^2 + p_{iz}^2 - a_2^2 - a_3^2}{2a_2a_3}\right), \tag{4} $$

$$ \theta_{i2} = \pm\left[\sin^{-1}\left(\frac{-a_3s_3}{\sqrt{(p_{ix}c_1 + p_{iy}s_1 - a_1)^2 + p_{iz}^2}}\right) - \varphi_i\right], \tag{5} $$

$$ \varphi_i = \tan^{-1}\left(\frac{p_{iz}}{p_{ix}c_1 + p_{iy}s_1 - a_1}\right). \tag{6} $$

For fore legs (i = 1, 2), θ_{i2} are positive and θ_{i3} are negative. Conversely, θ_{i2} are negative and θ_{i3} are positive for rear legs (i = 3, 4).

If given the coordinates of one foot in $\{O_b\}$, we can get its coordinates in $\{O_{i0}\}$ first by the inverse transformation of Eq. (1), then get the three joint variables θ_{ik} from Eqs. (3)-(6).

4. Foot trajectory planning

To minimize the contact forces between ground and the foot, the foot trajectory should meet the demand that velocity and acceleration become zero at the time of touchdown, liftoff and maximum foot height. The composite cycloid foot trajectory meets the demand well [15]. But it also has a serious defect that is the obvious relative slippage between feet and ground at the landing moment. The defect has been verified in experiments with a physical robot. A new ellipse-based trajectory generation method for galloping quadruped robot is proposed in Ref. [16].

This paper gives a composite foot trajectory composed of cubic curve for swing phase and straight line for stance phase with respect to torso fixed frame $\{O_b\}$. The foot trajectory meets the requirements that the velocities along z axis of the feet become zero at the moment of touchdown and liftoff and there are no fluctuations with the velocities of the torso along z and x axes. The equations for foot trajectory are

$$ x_{sw}(t) = \delta b + L\times\left(-\frac{16}{T^3}t^3 + \frac{12}{T^2}t^2 - \frac{1}{T}t - \frac{1}{4}\right), \tag{7} $$

$$ z_{sw}(t) = -H_b + H_f\times\left(-\frac{128}{T^3}t^3 + \frac{48}{T^2}t^2\right), \tag{8} $$

$$ x_{st}(t) = \delta b + L\times\left(-\frac{1}{T}t + \frac{1}{4}\right), \tag{9} $$

$$ z_{st}(t) = -H_b \tag{10} $$

where L represents stride length, T represents cycle time, t represents the remainder of simulation time divided by cycle time T, H_b and H_f represent the z coordinate of torso and the maximum foot height with reference to the ground, respectively.

Eqs. (7) and (8) represent the position variations of one foot along x and z axes during the swing phase, while Eqs. (9) and (10) represent its position variations during stance phase. Figs.

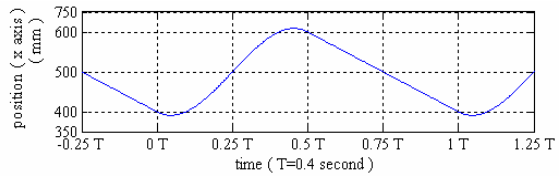

(a)

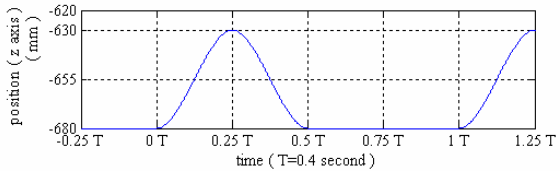

(b)

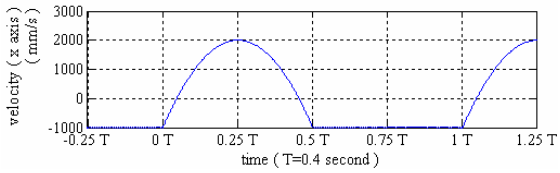

(c)

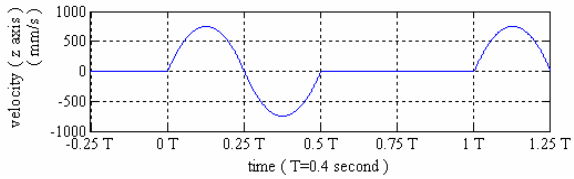

(d)

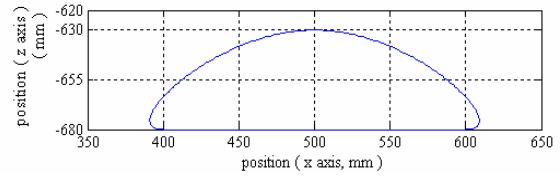

(e)

Fig. 4. Foot motions with respect to torso fixed frame $\{O_b\}$: (a) and (b) show the position variations along x and z axes, (c) and (d) show the velocity variations along x and z axes, (e) shows foot trajectory during one cycle time. (L = 400 mm, T = 0.4 s, H_f = 50 mm, H_b = 680 mm)

4(a) and 4(b) show the position variations of one foot along x and z axes in one cycle time, while Figs. 4(c) and 4(d) show its velocity variations. Fig. 4(e) shows the closed foot trajectory with respect to torso fixed frame $\{O_b\}$ during one cycle time.

According to Eqs. (9) and (10), the foot position variations with respect to torso fixed frame are constant along the z axis and linear along the x axis during stance phase. In other words, the position variations of the torso relative to ground are constant along the z axis and linear along the x axis under the assumption that there are no slippages between the supporting feet and ground. Fig. 5 shows the ideal position variations of torso along the x and z axes, respectively. From Eq. (9) or Fig. 5(a) it can be concluded that there exists a speed jump at the

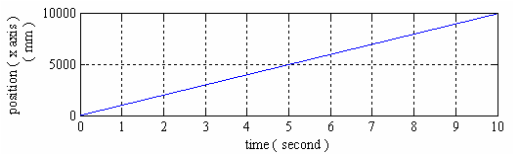

(a)

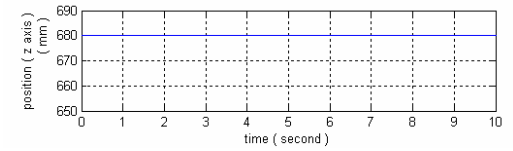

(b)

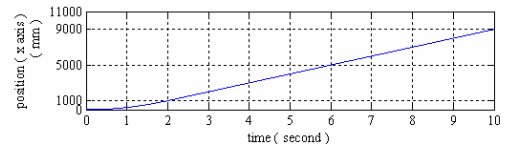

(c)

Fig. 5. Torso motion: (a) and (b) show the ideal position variations of torso along x and z axes with respect to ground fixed frame, respectively, (c) shows the ideal position variation of torso along x axis with a ramp accelerating stage.

start of the robot, so there exists greater inertial impact force too. If the robot starts with a ramp accelerating stage as shown in Fig. 5(c), the inertial force is very limited.

5. Dynamics simulation with MSC.ADAMS

To verify kinematic equations and the performance of the foot trajectory, and get some important parameters, dynamic simulations are made based on ADAMS. Since it is difficult to implement complex joint motion driving in ADAMS, MATLAB/Simulink is selected to make co-simulations with ADAMS [17]. Figs. 6 and 7 show the virtual prototype in ADAMS and co-simulation model in MATLAB of Scalf-1, respectively.

In co-simulation, the foot trajectory can be discretized to a series of points firstly. Then the coordinates of each point are substituted into the inverse kinematic equations to get all joint variables. Further, the displacements of hydraulic cylinders with respect to joint variables can be calculated according to the mechanical structure parameters of legs. As shown in Fig. 7, all the calculations are implemented in MATLAB and the cylinders displacements are transferred to ADAMS_SUB module as input variables to drive corresponding cylinders. The simulation results not only can be returned to MATLAB from ADAMS_SUB, but also can be processed in ADAMS postprocessor module. The coefficient of friction between supporting feet and ground is about 0.4 [18]. This and other parameters are listed in Table 3. Figs. 8 to 11 show parts of the simulation results.

From Fig. 8, it can be concluded that the kinematic equations are right and the cubic curve and straight line foot trajectory has higher performance than the composite cycloid foot trajectory.

Table 3. Parameters in simulation.

Parameters	Values
Payload	100 kg
Coefficient of friction	about 0.4
Locomotion gait	trot
Cycle time	0.4 s
Stride length	400 mm
Max foot height	50 mm
Accelerating time	2 s
Simulation step size	0.01 s
Simulation time	10 s

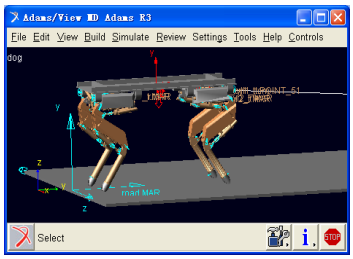

Fig. 6. Virtual prototype of Scalf-1 in MSC.ADAMS.

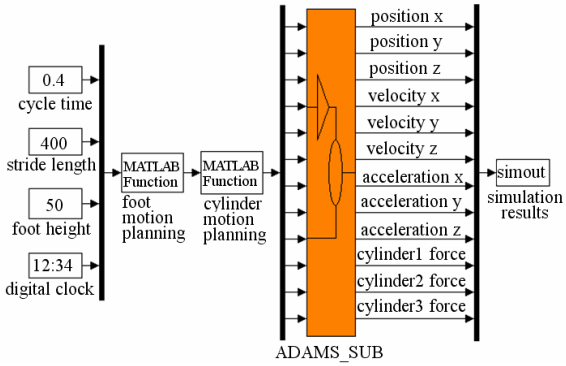

Fig. 7. Co-simulation model of Scalf-1.

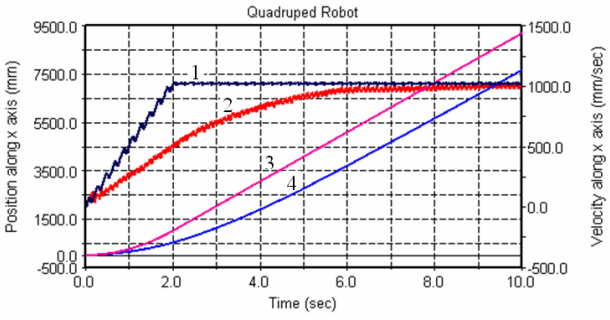

Fig. 8. Position and velocity variations of torso along *x* axis: curves 1 and 3, show the velocity and position variations of the torso in simulation with cubic curve and straight line foot trajectory, respectively, curves 2 and 4 show the velocity and position variations of the torso in simulation with composite cycloid foot trajectory, respectively.

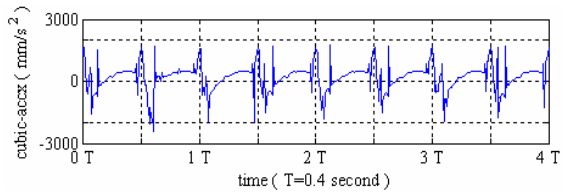

(a)

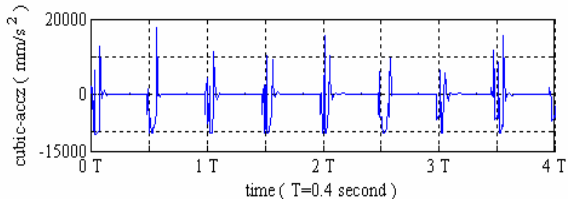

(b)

Fig. 9. The acceleration variations of torso: (a) and (b) show the acceleration variations along *x* and *z* axes, respectively.

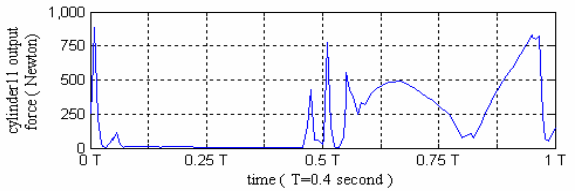

(a)

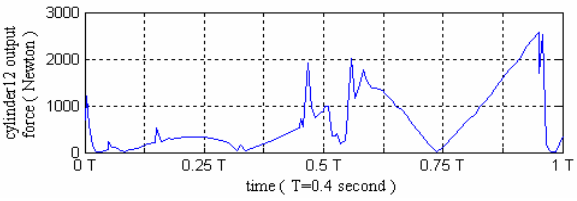

(b)

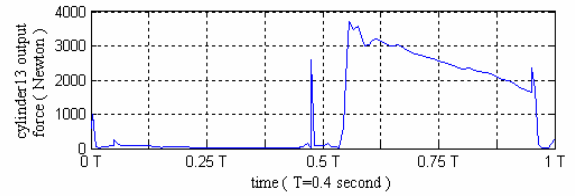

(c)

Fig. 10. Driving forces of three hydraulic cylinders of one leg during one cycle time.

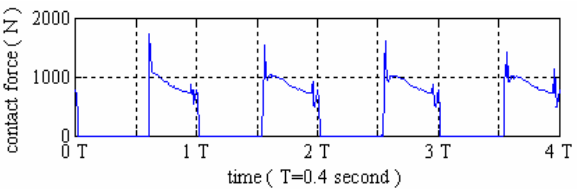

Fig. 11. Contact force between one foot and ground.

There are almost no slippages between the supporting feet and ground while Scalf-1 is running with cubic curve and straight line foot trajectory. The curve 3 is almost identical to the curve shown in Fig. 5(c). In contrast, there are obvious slippages while the robot is running with composite cycloid foot trajectory. The ideal accelerations of torso along x and z axes should be zero according to Figs. 5(a) and 5(b). As shown in Fig. 9, they are not zero in simulation since the actual shapes of four feet are not ideal points. The acceleration makes the velocity of the torso fluctuate slightly around the ideal velocity along x and z directions. This is the reason why the velocity variation curves 1 and 2 shown in Fig. 8 are not smooth.

Fig. 10 shows the output forces of three hydraulic cylinders of the same leg during one cycle time. It can be seen that the maximum driving force for all joints is about 3700 N. This means that the hydraulic cylinders must have the ability to output dynamic force of 3700 N. From Fig. 11, it can be concluded that the maximum impact force is about 1600 N, while the Scalf-1 is trotting with 100 kg payload. The impact force variation is consistent with that of the acceleration along the z axis shown in Fig. 9(b). Dynamic simulation results provide important references to the design of Scalf-1, such as:

- The maximum dynamic output force of cylinders.
- The maximum impact force between feet and ground.
- The optimal stride frequency.
- The stability of different foot trajectories.

6. Experiments

Many experiments upon payload capability, maximum velocity, gait transition, different ground adaptability etc., have been done with the physical prototype inside the laboratory [19]. The driving power is provided by a stationary hydraulic power pack driven by an AC electric motor. In the early stage of the development of Scalf-1, each hydraulic servo cylinder was controlled by a position servo controller. All servo controllers are connected to one onboard computer which communicates to the console computer through wireless protocol. The control architecture is shown in Fig. 12. Force feed back control is under research and will be applied to Scalf-1 in the near future. Figs. 13 and 14 show the payload capability and soil ground adaptability experiments, respectively. Fig. 15 shows the acceleration variations of torso along x and z axes. The parameters in experiments are the same in simulation as listed in Table 3.

The acceleration variations along the x and z axes measured by a gyro in one of the experiments are shown in Fig. 15. The acceleration along the z axis includes gravity acceleration. The variations are cyclical and the frequency is two times of stride frequency. Compared to Fig. 9, the acceleration variations amplitudes are almost identical, but the curves in Fig. 15 are smoother than the curves in Fig. 9 since the high frequency variations of acceleration have been filtered out by the gyro.

The experiments verified most of the simulation results and showed that the most stable locomotion gait is the trot and the optimal stride frequency ranges from 2 to 3 Hz for Scalf-1. The maximum velocity of the robot reaches 1.8 m/s running with trot gait on flat concrete ground and the payload capability exceeds 80 kg with the trotting velocity no less than 0.4 m/s.

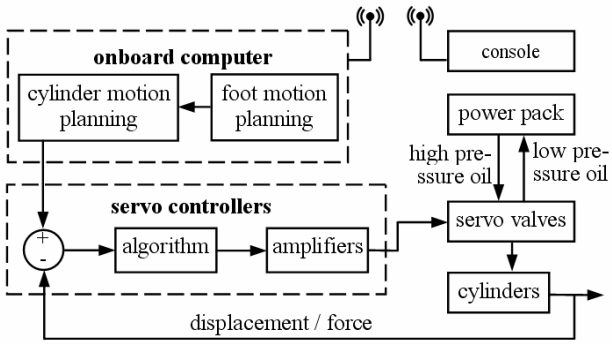

Fig. 12. Control architecture of Scalf-1.

Fig. 13. Scalf-1 trotting with 80 kg payload at 0.4 m/s.

Fig. 14. Scalf-1 trotting on soil ground at 0.4 m/s.

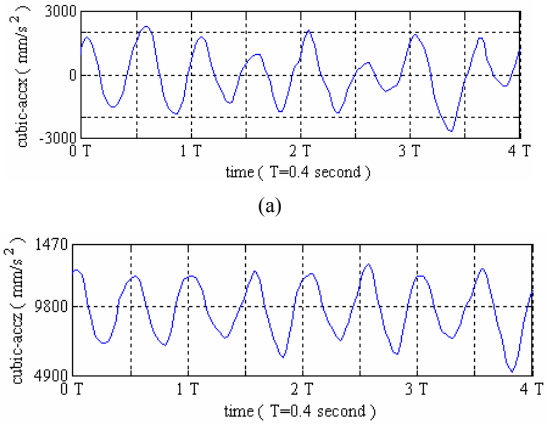

Fig. 15. The acceleration variations of torso in experiment: (a) and (b) show the acceleration variations along x and z axes respectively.

7. Conclusions

This paper describes a quadruped robot configuration driven by linear hydraulic servo cylinders and a composite foot trajectory composed of cubic curve and straight line. The composite foot trajectory makes Scalf-1 more stable in simulations and experiments than others. Trot gait and 2.5 Hz are the most stable locomotion gait and stride frequency verified by dynamic simulations and experiments. The maximum driving force of all joints and the maximum impact force between feet and ground in simulation provide important references for designing the physical prototype of Scalf-1.

In future work, we will design a miniaturized hydraulic power pack which is driven by an internal combustion engine, force feedback controller, add more sensors such as foot multi-axis force sensors, gyro etc. Then do more simulations and experiments.

Acknowledgment

This work is supported by the Independent Innovation Foundation of Shandong University with grant no. 2009JC010 and The High Technology Research and Development Program of China with grant no. 2011AA041001.

References

[1] S. M. Song and K. J. Waldron, *Machines that walk: The adaptive suspension vehicle*, MIT Press, Cambridge (1989).

[2] K. Berns and W. Ilg, Mechanical construction and computer architecture of the four-legged walking machine BISAM, *ASME Transactions on Mechatronics*, 4 (1) (1999) 32-38.

[3] C. Ridderstom and J. Ingvast, Quadruped posture control based on simple force distribution-a notion and a trial, *IEEE Conferrnce on Intelligent Robots and Systems,* Mad, Hawaii, USA (2001) 2326-2331.

[4] L. R. Palmer III and D. E. Orin, Quadrupedal running at high speed over uneven terrain, *Proceedings of the IEEE/RSJ Conference on Intelligent Robots and Systems*, San Diego, USA (2007) 303-308.

[5] H. Kimura, Y. Fukuoka and A. H. Cohen, Adaptive dynamic walking of a quadruped robot on irregular terrain based on biological concepts, *The International Journal of Robotics Research*, 22 (3-4) (2003) 187-202.

[6] J. W. Chung, I. W. Park and J. H. Oh, On the design and development of a quadruped robot platform, *Advanced Robotics*, 24 (2010) 277-298.

[7] T. J. Kim, B. So, O. Kwon and S. Park, The energy minimization algorithm using foot rotation for hydraulic actuated quadruped walking robot with redundancy, *the 6th German Conference on Robotics*, Munich, Germany (2010) 786-791.

[8] C. Semini, HyQ - Design and development of a hydraulically actuated quadruped robot, *PhD dissertation*, University of Genoa, Italy (2010).

[9] M. Raibert, K. Blankespoor and G. Nelson et al., Bigdog, the rough-terrain quadruped robot, *International Federation of Automation Control*, Seoul, Korea (2008).

[10] X. W. Rong, Y. B. Li, J. H. Ruan and H. J. Song, Kinematics analysis and simulation of a quadruped robot, *Applied Mechanics and Materials*, 26-28 (2010) 517-522.

[11] K. T. Stranga and K. Teudel, Explaining the scaling of transport costs: the role of stride frequency and stride length, *Journal of Zoology*, 221 (1990) 343-358.

[12] N. C. Heglund and C. R. Taylor, Speed, stride frequency and energy cost per stride: how do they change with body size and gait? *Journal of Experimental Biology*, 138 (1988) 301-318.

[13] N. C. Heglund, C. R. Taylor and T. A. McMahon, Scaling stride frequency and gait to animal size: Mice to horses, *Science*, 186 (4169) (1974) 1112-1113.

[14] R. P. Paul, *Robot manipulators: Mathematics, programming, and control*, MIT Press, Cambridge (1981).

[15] Y. Sakakibara, K. Kan, Y. Hosoda and M. Hattori et al., Foot trajectory for a quadruped walking machine, *IEEE International Workshop on Intelligent Robots and Systems*, Ibaraki, Japan (1990) 315-322.

[16] K. Y. Kim and J. H. Park, Ellipse-based leg-trajectory generation for galloping quadruped robots, *Journal of Mechanical Science and Technology*, 22 (2008) 2099-2106.

[17] MSC.Software, *MSC.ADAMS/VIEW advanced training guide*, Tsinghua University Press, Beijing (2004).

[18] F. Lin, Y. D. S. Zhang and X. D. Ma, Study on the friction characteristics of polyurethane for the friction liner of hoisting, *Lubrication Engineering*, 2 (2000) 33-35.

[19] Video information about quadruped robot from the website of the Robotics Research Center of Shandong University. http://www.sucro.org/ShowNews.asp?id=3782.

Xuewen Rong received his Bachelor and Master's degrees from Shandong University of Science and Technology, China, in 1996 and 1999, respectively. He is currently a senior engineer and a graduate student of the PhD course also in the School of Control Science and Engineering, Shandong University, China. His research interests include robotics, mechatronics, and hydraulic servo driving technology.

Yibin Li received his Bachelor and Doctoral degrees from Tianjin University, China, in 1982 and 2006, respectively. He received his Master's degree from Shandong University of Science and Technology, China, in 1988. He is currently a professor and associate dean in the School of Control Science and Engineering, Shandong University, China. His research interests include robotics, mechatronics, intelligent control, and intelligent vehicles.